Supporting Information

Latham et al. 10.1073/pnas.1322079111

SI Materials and Methods

Glycerol and Sucrose Viscogen Titrations. Two 500-μL α_7 samples were used for each viscogen titration. Initially, sample 1 contained α_7 in NMR buffer (25 mM potassium phosphate at pH 6.8, 50 mM NaCl, 1 mM EDTA, 0.02% (wt/vol) NaN_3 in 99% ^2H_2O) and sample 2 comprised α_7 in NMR buffer with 25% (vol/vol) glycerol [25% (wt/vol) sucrose]. The two initial samples were prepared by diluting 250 μL of twofold-concentrated α_7 with equal parts buffer plus 10 mM tryptophan or 2× viscogen [i.e., 50% (vol/vol) glycerol or 50% (wt/vol) sucrose] plus 10 mM tryptophan in NMR buffer. For each point in the titration, equal aliquots were removed from each sample and replaced with the aliquot from the other sample. In this way, the viscogen concentration of the first sample (buffer) increased whereas the viscogen concentration of the second sample (25% viscogen) decreased, with the concentration of α_7 remaining constant. This process was repeated in 2.5% viscogen steps until both samples were 12.5% viscogen, resulting in 13 titration points, with NMR experiments recorded on both 12.5% viscogen samples.

***Thermus thermophilus* Lysate Samples.** *T. thermophilus* lysate was prepared by growing HB8 cells (ATCC no. 27634) in media containing 0.8% (wt/vol) polypeptone, 0.4% (wt/vol) yeast extract, and 0.2% (wt/vol) NaCl at 70 °C until OD_{600} ~1.0. The cells were separated from the media, resuspended in 25 mL ^2H_2O, and lysed, and the insoluble material was spun down. Then, 5 mM benzamidine, 0.1 mg/mL PMSF, and 0.02% (wt/vol) NaN_3 were added to the lysate before sterile filtration through a 0.22-μm syringe filter. The total protein concentration of all lysate samples was determined by Bradford assay (Bio-Rad).

Small molecules (<3 kDa) from the lysate were obtained by concentrating sterile filtered lysate from 1 L of *T. thermophilus* culture in a 3-kDa molecular weight cutoff (MWCO) Amicon centrifugal concentrator. The flow-through then was dried down in a speed vacuum. The small molecules were reconstituted into a 500-μL sample of α_7 in three steps used in the titration.

A stock containing only the macromolecular fraction (>6 kDa) from the lysate was prepared by extensively dialyzing the lysate from 1 L of *T. thermophilus* culture (~30 mL) against 3× 4L 25 mM potassium phosphate (pH 6.8), 50 mM NaCl, 1 mM EDTA, 0.02% (wt/vol) NaN_3 at 4 °C. The dialyzed lysate then was buffer exchanged into NMR buffer and concentrated using a 3-kDa MWCO Amicon centrifugal concentrator. The 100-g/L protein sample was made by diluting a suitable amount of concentrated lysate to 500 μL with concentrated α_7 and NMR buffer. Samples at 150 g/L and 200 g/L subsequently were made through the addition of the appropriate amount of concentrated lysate, with subsequent concentration of the sample back to a volume of 500 μL.

The 100-g/L complete lysate sample was prepared by concentrating sterile filtered lysate from 1 L of *T. thermophilus* in a 3-kDa MWCO Amicon centrifugal concentrator. The flow-through then was dried down in a speed vacuum and reconstituted in a small volume of ^2H_2O, which was added back to the concentrated lysate. In this way, the lysate contained all macromolecules and small molecules from the original diluted sample. The appropriate amount of concentrated lysate then was diluted to 100 g/L lysate protein.

The small molecule probes used in viscosity measurements included ^{13}C-labeled methanol, 1-^{13}C ethanol, 2-^{13}C isopropanol, 2-^{13}C glycerol, 1-^{13}C ribose, and sucrose (glucose sugar labeled as $^{13}C_6$) and were gifts from Cambridge Isotope Laboratories Inc. Along with 2-^{13}C acetate, 0.5-M stock solutions of these molecules were prepared by reconstituting into NMR buffer. Appropriate volumes were added to two 100-g/L *T. thermophilus* complete lysate samples to obtain small molecule concentrations of 2.5 and 10 mM. A similar sample also was prepared in NMR buffer at a small molecule concentration of 10 mM.

NMR Spectroscopy. NMR data were acquired at 45 °C on Varian Inova 11.7 T [500 MHz ^{1}H(ν)] and 14.0 T [600 MHz ^{1}H(ν)] spectrometers equipped with standard triple-resonance and cryogenically cooled triple-resonance gradient probes, respectively. The sample temperature was calibrated using a thermocouple placed inside an NMR tube.

(*i*) Diffusion: Residual HDO and tryptophan translational diffusion coefficients were measured using a modified 1D convection-compensated stimulated echo longitudinal encode decode (sLED) pulsed-field gradient NMR experiment that is very similar to the scheme described in figure 1B of Zheng and Price (1), whereas α_7 translational diffusion coefficients were obtained similarly, using a modified 1D ^{13}C-edited version of the experiment. For each dataset, two experiments were performed with diffusion delays of either 100 or 200 ms and 11 dephasing/rephasing gradients with strengths ranging from 4 to 60 G/cm (1 ms duration).

Diffusion coefficients of small molecule probes dissolved in buffer or lysate also were measured at 45 °C by using a convection-compensated 2D ^{13}C, ^{1}H correlation pulse sequence (available upon request). ^{13}C decoupling was not used during acquisition to prevent sample heating. Gradient strengths were varied from 10 to 30 G/cm, with a gradient duration of 1 ms and a diffusion delay of 100 ms.

(*ii*) Magnetization exchange: Spectra were acquired using a ^{13}C-edited scheme in which a mixing element was inserted between t_1 and t_2 evolution periods, as described previously (2, 3). During the mixing time, longitudinal order, $2I_ZC_Z$, evolves, where A_Z is the Z component of A magnetization. The use of longitudinal order, as opposed to ^{1}H Z-magnetization during this element, eliminates NOE correlations that otherwise would be observed. The result is a series of 2D ^{1}H,^{1}H spectra recorded as a function of parametrically varied mixing-time delays (in this case, 13 values between 0.01 and 1 s, with two delay times repeated for error analysis). Spectra were collected with acquisition times of 100 and 80 ms (72 × 640 complex points) in the t_1 and t_2 dimensions, respectively.

The effects of differential transverse relaxation of magnetization from each of the states during the insensitive nuclei enhanced by polarization transfer (INEPT) delays in the magnetization transfer experiment were taken into account, as described below, using ^{1}H R_2 values measured using a modified 2D ^{13}C,^{1}H heteronuclear single quantum coherence (HSQC) experiment. Pseudo-3D experiments were acquired with four relaxation delays between 1.8 and 15.9 ms.

Populations of each of the interconverting states, which are required in fits of magnetization exchange datasets, were determined from the average of peak intensities measured in two to four 2D ^{13}C,^{1}H HSQC spectra. An interscan delay of 3 s was used to ensure that fully relaxed spectra were analyzed. Acquisition times of 60 and 80 ms were used in the t_1 and t_2 dimensions, respectively.

All NMR datasets were processed and visualized with the NMRPipe/NMRDraw software suite (4).

Determination of Solution Viscosities. Viscosities used in the analysis of $k_{m\to n}$ vs. η profiles were calculated from measured translational diffusion coefficients of HDO, tryptophan, and α_7

probe molecules, which in turn, were obtained by fitting intensities of probe peaks as a function of dephasing/rephasing gradient strengths to equation 8 of Zheng and Price (1) (Fig. S3). In general, diffusion coefficients were measured with two diffusion delays to ensure that convection was compensated properly by the NMR experiment (1), with differences of less than 2%. Values of η were calculated from the Stokes–Einstein equation, $D=\frac{k_bT}{6\pi\eta R_H}$, using R_H = 1.12, 3.88, and 63.3 Å for HDO, tryptophan, and α_7, respectively. These values of R_H, in turn, were obtained by measuring diffusion coefficients of HDO, tryptophan, α_7, and dioxane simultaneously (same solution) before the addition of viscogen, using the reported value of R_H for dioxane (2.12 Å) (5) and the relation $R_{H,probe}=R_{H,Dioxane}\frac{D_{Dioxane}}{D_{probe}}$.

The analysis described above makes use of the Stokes–Einstein equation with stick boundary conditions, which has been shown to be appropriate for cases in which the solute is highly solvated (6). We also determined viscosities of probe molecules using an alternative approach that bypasses the Stokes–Einstein equation. The viscosity of a dilute solution of probe molecules can be well approximated by the viscosity of pure solvent (D_2O), which is tabulated as a function of temperature. Using a tabulated value of η_{D2O}= 0.76 cP (45 °C), the viscosity of a viscogen solution, as measured by the diffusion of a probe molecule (η_{probe}), can be calculated from the diffusion constants of the probe in a buffer-only sample ($D_{probe,buffer}$) and in viscogen ($D_{probe,viscogen}$) solutions as $\eta_{probe}=\eta_{D2O}\frac{D_{probe,buffer}}{D_{probe,viscogen}}$. Fig. S5 shows correlation plots between η_{probe} values measured both ways for water and tryptophan probe molecules, and the agreement is excellent.

To construct the molecular ruler of Fig. 4*C* of the text, values of $\frac{\eta^*_{probe}}{\eta_{buff}}$, the ratio of the viscosities of lysate (η^*_{probe}) and buffer (η_{buff}) solutions as measured by a probe of hydrodynamic radius $R_{H,probe}$, have been determined. These were obtained by fitting intensity vs. gradient profiles from diffusion experiments, as $I=I_0\exp(-dg^2)$, where d is the diffusion decay rate, proportional to the diffusion coefficient D, and g is the dephasing/rephasing gradient strength. It follows that $\frac{\eta^*_{probe}}{\eta_{buff}}=\frac{D_{probe,buff}}{D_{probe,lysate}}=\frac{d_{probe,buff}}{d_{probe,lysate}}$. Values of $R_{H,probe}$ were obtained from the relation $R_{H,probe}=\frac{d_{acetate,buff}}{d_{probe,buff}}R_{H,acetate}$ using $R_{H,acetate}$ = 2.24 Å (7).

Analysis of Magnetization Exchange Data. Exchange rate constants were determined by simultaneously fitting the time dependencies of auto- and cross-peaks for M-1 measured in a set of magnetization exchange datasets, as described in detail previously (3). We chose to carry out all exchange experiments described in this work at 45 °C. Samples of α_7 are stable until ∼50 °C, and at lower temperatures, the contributions to the linewidths of M-1 correlations in ^{1}H-^{13}C spectra from chemical exchange become significantly more pronounced (8), complicating the extraction of accurate rates, especially as a function of increasing solution viscosity.

The time dependence of magnetization exchange is given by Eq. **S1** as

$$M_{m\to n}(t)=\lambda\vec{v}_n\ \exp(\mathbf{K}t)\vec{p}_m, \qquad \textbf{[S1]}$$

where λ corresponds to the total magnetization at t = 0, $\vec{v}_n=\{[1\quad 0],[0\quad 1]\}$, $\vec{p}_m=\left\{\begin{bmatrix}p_{out}\\0\end{bmatrix},\begin{bmatrix}0\\p_{in}\end{bmatrix}\right\}$, and p_{out}, p_{in} are the fractional populations at equilibrium estimated from peak intensities in 2D ^{13}C,^{1}H HSQC spectra. **K** is the exchange matrix given by

$$\mathbf{K}=\begin{bmatrix}-k_{out\to in}-R_{ZZ,out} & k_{in\to out}\\ k_{out\to in} & -k_{in\to out}-R_{ZZ,in}\end{bmatrix}, \qquad \textbf{[S2]}$$

where $k_{m\to n}$ is the rate constant for exchange from state m to n and $R_{ZZ,n}$ is the relaxation rate of longitudinal order ($2I_ZC_Z$, see above) of state n.

As summarized in the text and described in detail below (*Justification of Two-State Analysis*), we have analyzed our data in the context of a two-site exchange mechanism involving the "out" state (state A) and a composite "in" state (corresponding to state B + state C). Such an analysis was necessitated because of the small ^{1}H$^\varepsilon$ shift difference between M-1 of states B and C and the resultant peak broadening that accompanies studies in viscogens, which does not allow the separate quantification of B–C and C–B cross-peaks.

Intensities of diagonal and cross-peaks were obtained via "box sums," implemented with NMRGlue (9). Before fitting of the data, peak intensities were corrected for differential ^{1}H R_2 relaxation during INEPT transfers (R_2 values of ∼7 and ∼37 s^{-1} for out and in states, respectively; buffer sample) by using ^{1}H transverse relaxation rates that were measured in separate experiments (see above). Fits were performed with in-house software (available upon request), with errors determined from a jackknife procedure (10).

Equilibrium populations of each of the states, p_{out} and p_{in}, were calculated from peak volumes obtained from fits of fully relaxed 2D ^{13}C,^{1}H HSQC spectra, corrected for the differential loss of magnetization during INEPT transfers, as described above.

Calculation of Internal Friction Values. Values of σ were calculated from fits of Eq. **1** to profiles of exchange rate constants $k_{m\to n}$ vs. η via minimization of a χ^2 target function, $\chi^2=\sum_\eta\frac{(k_{obs(\eta)}-k_{calc(\eta)})^2}{\sigma^2_{SD,\eta}}$, where $k_{obs(\eta)}$ and $k_{calc(\eta)}$ are the experimental and back-calculated $k_{m\to n}$ values at each viscosity (η), respectively, and $\sigma^2_{SD,\eta}$ is the variance of the experimental error in k_{obs}. Errors in the reported σ values were obtained from 500 bootstrap simulations (10).

SI Text

Justification of Two-State Analysis. As discussed in detail in a previous publication (3), exchange of gating residues in the proteasome can be well described in terms of a three-site interconversion process involving an out state (state A, corresponding to the case in which the gates are localized above the lumen of the proteasome barrel) and a pair of in conformations (states B and C, in which the gates are within the lumen). Magnetization exchange then is given by a coupled set of equations:

$$\begin{aligned}\frac{d}{dt}M_A&=-(R_{ZZ,A}+k_{AB}+k_{AC})M_A+k_{BA}M_B+k_{CA}M_C\\ \frac{d}{dt}M_B&=k_{AB}M_A-(R_{ZZ,B}+k_{BA}+k_{BC})M_B+k_{CB}M_C\\ \frac{d}{dt}M_C&=k_{AC}M_A+k_{BC}M_B-(R_{ZZ,C}+k_{CA}+k_{CB})M_C,\end{aligned} \qquad \textbf{[S3]}$$

where $R_{ZZ,m}$ and k_{mn} are defined as above and M_i is the magnetization (two spin order) from state i. Eq. **S3** can be simplified by noting that $k_{ij}p^o_i=k_{ji}p^o_j$ so that the fitting values include three decay rates $\{R_{ZZ,i}\}$ and three exchange rates $\{k_{ex,ij}=k_{ij}+k_{ji}\}_{i\neq j}$, with equilibrium values of fractional populations of each state, p^o_i, measured from peak intensities in ^{13}C,^{1}H correlation spectra. These six values may be obtained from fits of diagonal and cross-peaks in magnetization exchange datasets recorded as a function of a parametrically varied delay during which chemical exchange occurs. Central to the analysis described above is that the correlations for all diagonal and cross-peaks are well resolved in magnetization exchange spectra so that peak intensities may be quantified properly. Resolution is limiting in the present study because (*i*) ^{13}C chemical shifts of M-1 from states A, B, and C are within 0.048 ppm and (*ii*) M-1 ^{1}H lines of states B and C are

separated by only 0.059 ppm. The proximity of ^{1}H shifts in states B and C leads to overlap between diagonal and cross-peaks, severely complicating analysis using a three-site exchange model, especially for experiments recorded with increasing amounts of viscogen, which results in significant line broadening. Thus, we chose to combine states B and C in the analysis by noting that

$$\begin{aligned}\frac{d}{dt}M_A &= -\left(R_{ZZ,A}+k_{AB}+k_{AC}\right)M_A+\left(\frac{k_{BA}+k_{CA}}{2}\right)(M_B+M_C)\\ &\quad+\left(\frac{k_{BA}-k_{CA}}{2}\right)(M_B-M_C)\\ \frac{d}{dt}(M_B+M_C) &= (k_{AB}+k_{AC})M_A\\ &\quad-\left(\frac{R_{ZZ,B}+R_{ZZ,C}+k_{BA}+k_{CA}}{2}\right)(M_B+M_C)\\ &\quad-\left(\frac{R_{ZZ,B}-R_{ZZ,C}+k_{BA}-k_{CA}}{2}\right)(M_B-M_C).\end{aligned}$$

[S4]

Eq. **S4** is no less general than Eq. **S3**; however, it may be simplified in the case of the gating kinetics quantified here. First, equilibrium values of p_B and p_C, 16 ± 1% and 18 ± 0.3%, are essentially the same to within error, as are values of $R_{ZZ,B}$ and $R_{ZZ,C}$. Second, from an analysis of exchange data recorded in buffer (3), k_{BA} ~0.23 s^{-1} and k_{CA} ~0.14 s^{-1}, which also are similar. Thus, the final term in each of the equations in Eq. **S4** is significantly smaller than the others and, as we show below, may safely be neglected. In this case, Eq. **S4** reduces to the standard set of coupled equations describing a two-site exchange process, out (A) ⇔ in (B + C):

$$\begin{aligned}\frac{d}{dt}M_{out} &= -\left(R_{ZZ,out}+k_{out\to in}\right)M_{out}+k_{in\to out}M_{in}\\ \frac{d}{dt}M_{in} &= k_{out\to in}M_{out}-\left(R_{ZZ,in}+k_{in\to out}\right)M_{in},\end{aligned}$$

[S5]

with $M_{out} = M_A$, $M_{in} = M_B + M_C$, $R_{ZZ,out} = R_{ZZ,A}$, $R_{ZZ,in} = 0.5\,(R_{ZZ,B} + R_{ZZ,C})$, $k_{out\to in} = k_{AB} + k_{AC}$, and $k_{in\to out} = \frac{k_{BA}+k_{CA}}{2}$.

To explore this simplification further, we carried out a series of computations. Here, we have taken values for exchange rates $(k_{AB}, k_{BA}, k_{AC}, k_{CA}, k_{BC}, k_{CB}) = (0.067, 0.231, 0.037, 0.141, 0.650, 0.720)$ s^{-1} that were measured previously from the analysis of exchange time profiles recorded on α_7 samples dissolved in buffer (3). Note that we have had to apply steep window functions to the data so as to resolve the diagonal and cross-peaks derived from states B and C. Because of differential linewidths, this process most certainly will introduce error into the extracted rates; hence, these rates should be considered preliminary. Here, we use them only to illustrate that the two-state approximation is valid. Using the rates given above, along with σ = 0.3 cP and η = 0.78 cP (viscosity of D_2O at 45 °C), values of $A_{m\to n}$ were calculated from Eq. **1**, and these were used to compute 13 sets of three-site exchange profiles (Eq. **S4**), one set for each of the η values of the glycerol titration. A two-site exchange model subsequently was fit to each set of profiles (Eq. **S5**), with the fitted $(k_{out\to in}, k_{in\to out})$ and input $(k_{AB}+k_{AC}, \frac{k_{BA}+k_{CA}}{2})$ rates plotted in Fig. S2 *A* and *B*. Excellent correlations are obtained, with Pearson's correlation coefficients of 0.999 for both plots and slopes of 0.99–1.0, validating the use of the two-site exchange model.

We also were interested in establishing whether accurate σ values were fit using this two-site exchange procedure. Calculations were performed as described above to generate sets of three-site magnetization exchange profiles (Eq. **S4**), with one set for each of 15 different σ values, spanning a range from 0.01 to 5 cP. Note that we assume that each of the six exchange rates that describe the three-site exchange process is given by Eq. **1** with the same σ value. Each set of profiles subsequently was fit to a two-site model (Eq. **S5**), and the extracted exchange rates vs. η profile was fit to Eq. **1** of the text to obtain σ. The process was repeated for each σ, and the results are plotted in Fig. S2*C*. An excellent correlation is obtained with a Pearson correlation coefficient of 0.999, and the slope of 0.94 indicates that σ values acquired in this manner are within ~6% of the correct values.

Measurement of Solution Viscosities. Solution viscosities have been obtained in two different ways, as described in *SI Materials and Methods*, and the agreement between the different approaches is excellent (Fig. S5). As described in the text, the viscosity dependence of exchange rates may be used to estimate the relative contributions of solvent and internal (intraproteasome) frictional forces to the process of gate interconversion. Fig. 3 plots exchange rate constants $k_{out\to in}$ and $k_{in\to out}$ as a function of solution viscosity, estimated by converting measured diffusion constants of water in the viscogen solutions to η via the Stokes–Einstein equation (*Materials and Methods*). The corresponding plot with solution viscosity calculated from the relative diffusion constants of water in solutions of viscogen and buffer, using the tabulated viscosity value for D_2O (45 °C) in buffer ($\eta_{D2O}\frac{D_{water,buffer}}{D_{water,viscogen}}$), is shown in Fig. S6. Notably, calculated σ values remain nearly identical irrespective of the way η is obtained.

A central issue in studies of the sort presented here concerns the choice of probe used to measure viscosity. The differences between micro- and macroscopic viscosities are well established (11, 12), and measured viscosities in solutions of viscogens may vary significantly with probe size, as shown in the present application. In the absence of knowledge of the effective hydrodynamic radius (EHR) of the reaction, as would be the case in any initial study, a small viscogen such as glycerol is critical. In this case, any probe molecule, from the size of water and upward, would report very similar viscosities that, in turn, are used as a proxy for the viscosity along the reaction coordinate (see text). This is not the case when larger viscogens, such as sucrose, are used. Fig. S4 plots diffusion coefficients of the probe molecules water and tryptophan as a function of the concentration of viscogen using either glycerol ($R_{H,v}$ = 2.6 Å) or sucrose ($R_{H,v}$ = 4.5 Å). For glycerol, the diffusion profiles are essentially independent of probe size. By contrast, tryptophan diffusion decreases more rapidly than water in sucrose solutions, reflecting the fact that the tryptophan probe ($R_{H,v}$ = 3.5 Å) reports on the macroscopic viscosity of the solution, whereas the small size of water relative to sucrose leads to a smaller viscosity estimate from this probe (microscopic viscosity).

As discussed in the text, very similar values of σ are obtained from viscosity estimates of glycerol solutions using water, tryptophan, or α_7 probes. This reflects the fact that all probes "sense" a macroscopic viscosity, and the length scale becomes unimportant. Accurate values of σ, independent of probe size, are obtained in this case. For viscogens such as sucrose, the measured solution viscosity is a function of probe size (Fig. S4) and σ values may be overestimated significantly, by a factor of ~3 for proteasome gating when η is calculated from the diffusion of tryptophan or α_7 (Fig. 3*C* in the text). It thus is clear that the macroscopic viscosity exceeds the viscosity along the reaction coordinate. To summarize, the EHR of an exchange process may be significantly smaller than the hydrodynamic radius of the molecule that is interconverting (α_7 in this case). The viscosity along the reaction coordinate, which depends on the EHR of the conformational transition, thus may be significantly smaller than the macroscopic solution viscosity when a large viscogen is used. For this reason, using the macroscopic viscosity as measured by a viscometer (as often is done in these studies) may lead to errors unless small viscogens are used.

Validity of the Molecular Ruler. Fig. 4*C* of the main text shows the molecular ruler we constructed correlating the increased viscosity (over buffer) of a probe molecule in *T. thermophilus* complete lysate (100 g/L lysate protein concentration) as a function of the hydrodynamic radius of the probe. Once the length scale of a kinetic process has been determined in buffer, it is possible to estimate the viscosity along the reaction coordinate in a lysate environment from Fig. 4*C* and, hence, the kinetics in lysate so long as the lysate acts as a "good" viscogen (i.e., there are no direct interactions with the system studied) and σ is known. The ruler is useful, however, only if the probes used to construct it also do not interact with the lysate components, because any binding interaction will decrease the measured η_{probe} values. To identify and eliminate such probes, we have performed several checks. First, the chemical shifts of the probes in buffer and lysate were compared. Probes whose chemical shifts or other spectral signatures (such as linewidths and relative peak intensities) differed in lysate were assumed to be either bound or chemically altered by lysate components and therefore were not included in the analysis. Based on this criterion, for example, 1-^{13}C glucose, α-ketobutyrate and α-ketoisovalerate were excluded from the molecular ruler. The ^{1}H and ^{13}C chemical shifts of the remaining probes correlate very well with values obtained in buffer (Fig. S8 *A* and *B*). In addition, diffusion coefficients in lysate were measured at probe concentrations of 2.5 and 10 mM. In the event there is no binding, the diffusion coefficients at both concentrations will be identical to within measurement error. On the other hand, in the event binding does occur, it is expected that the diffusion constant of the probe at 2.5 mM will be less than at 10 mM, because at the elevated concentration, a smaller fraction of the probe would be bound. Of course, it is possible that even at 10 mM, the probe is fully bound to a target in the ligand so that similar diffusion values would be obtained at probe concentrations of both 2.5 and 10 mM; however, this is unlikely given the concentrations of probe used. Fig. S8*C* shows that the diffusion coefficients of the probes used to construct the ruler, measured at concentrations of 2.5 and 10 mM, are very similar (except for a small systematic deviation toward faster diffusion coefficients for probes at 2.5 mM, opposite of what one expects for binding). Taken together, the chemical shift and diffusion results provide strong evidence that the small molecule probes used for analysis do not bind lysate components and, therefore, faithfully report on free diffusion.

1. Zheng G, Price WS (2009) Simultaneous convection compensation and solvent suppression in biomolecular NMR diffusion experiments. *J Biomol NMR* 45(3):295–299.
2. Sprangers R, Kay LE (2007) Quantitative dynamics and binding studies of the 20S proteasome by NMR. *Nature* 445(7128):618–622.
3. Religa TL, Sprangers R, Kay LE (2010) Dynamic regulation of archaeal proteasome gate opening as studied by TROSY NMR. *Science* 328(5974):98–102.
4. Delaglio F, et al. (1995) NMRPipe: A multidimensional spectral processing system based on UNIX pipes. *J Biomol NMR* 6(3):277–293.
5. Wilkins DK, et al. (1999) Hydrodynamic radii of native and denatured proteins measured by pulse field gradient NMR techniques. *Biochemistry* 38(50):16424–16431.
6. Schmidt J, Skinner J (2004) Brownian motion of a rough sphere and the Stokes-Einstein law. *J Phys Chem B* 108(21):6767–6771.
7. Chatterjee C, Martinez D, Gerig JT (2007) Interactions of trifluoroethanol with [val5] angiotensin II. *J Phys Chem B* 111(31):9355–9362.
8. Baldwin AJ, Religa TL, Hansen DF, Bouvignies G, Kay LE (2010) 13CHD2 methyl group probes of millisecond time scale exchange in proteins by 1H relaxation dispersion: An application to proteasome gating residue dynamics. *J Am Chem Soc* 132(32): 10992–10995.
9. Helmus JJ, Jaroniec CP (2013) Nmrglue: An open source Python package for the analysis of multidimensional NMR data. *J Biomol NMR* 55(4):355–367.
10. Press WH, Teukolsky SA, Vetterling WT, Flannery BP (2007) *Numerical Recipes 3rd Edition: The Art of Scientific Computing* (Cambridge Univ Press, New York).
11. Barshtein G, Almagor A, Yedgar S, Gavish B (1995) Inhomogeneity of viscous aqueous solutions. *Phys Rev E Stat Phys Plasmas Fluids Relat Interdiscip Topics* 52(1): 555–557.
12. Hołyst R, et al. (2009) Scaling form of viscosity at all length-scales in poly(ethylene glycol) solutions studied by fluorescence correlation spectroscopy and capillary electrophoresis. *Phys Chem Chem Phys* 11(40):9025–9032.

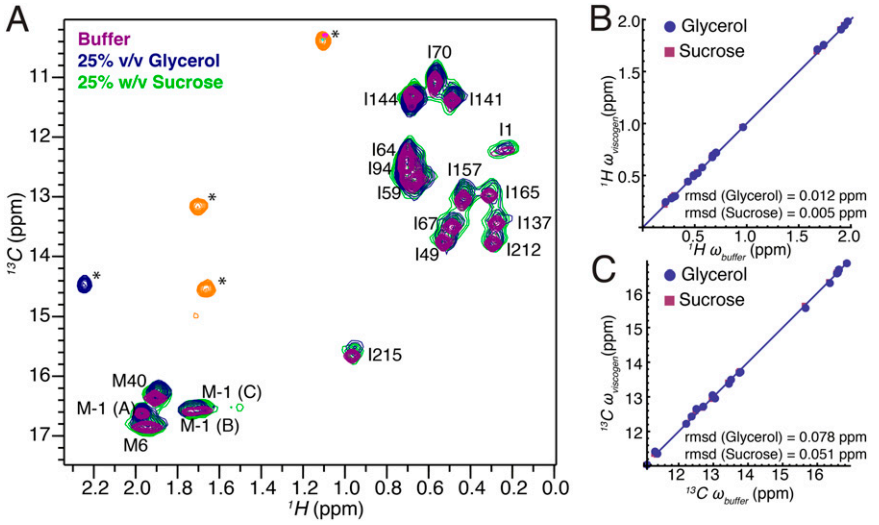

Fig. S1. The structure of α_7 is not perturbed by viscogen. (*A*) Two-dimensional ^{13}C,^{1}H HSQC spectra of U-^{2}H, $^{13}CHD_2$-M, $^{13}CHD_2$-I(δ1) M1I α_7 in buffer (purple contours), 25% (vol/vol) glycerol (blue contours), and 25% (wt/vol) sucrose (green contours) recorded at 14 T and 45 °C. Peak assignments are indicated; blue and orange (negative contoured) peaks denoted with asterisks result from a contaminant of the glycerol. Correlation plots of ^{1}H (*B*) and ^{13}C (*C*) Iδ1 and Mε methyl group chemical shifts in viscogen vs. buffer. The solid line is y = x, and the rmsd of α_7 methyl shifts in buffer and viscogen for each viscogen is given in the lower right corner.

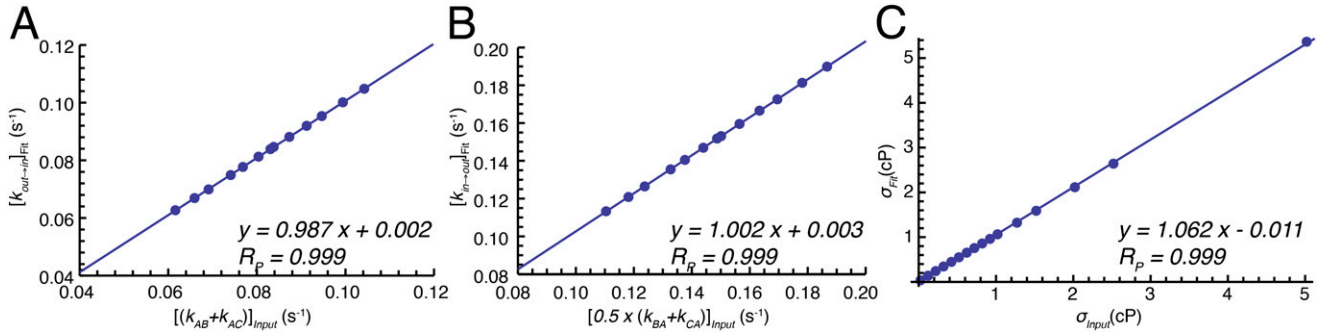

Fig. S2. Validation of the two-site exchange model used in the analysis of α_7 gating kinetics. (*A* and *B*) Correlation plots of fitted ($k_{out\rightarrow in}$) vs. input ($k_{AB} + k_{AC}$) (*A*) and fitted ($k_{in\rightarrow out}$) vs. input [$0.5 \times (k_{BA} + k_{CA})$] (*B*) values, as described in *SI Text*. (*C*) Correlation plot of fitted vs. input σ values. See *SI Text* for details.

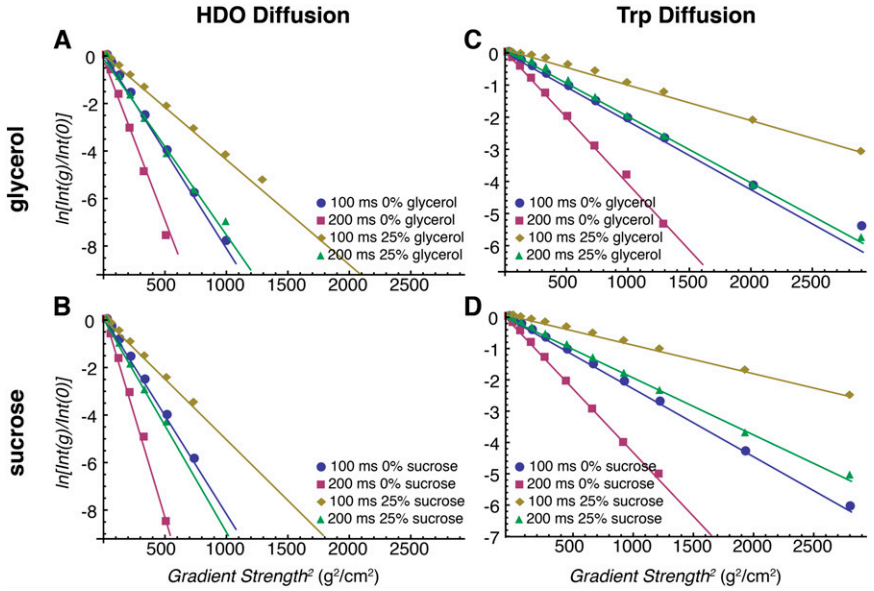

Fig. S3. Representative diffusion curves of probes (water, tryptophan) in solutions of viscogens, as measured by pulsed field gradient NMR at 45 °C. Plots of the logarithm of normalized peak intensities as a function of the square of the amplitudes of gradient encoding pulses are shown for HDO diffusion in glycerol (*A*) and sucrose (*B*) and tryptophan in glycerol (*C*) and sucrose (*D*). Lines are the best fit to the plotted data, where the slope is proportional to the diffusion coefficient.

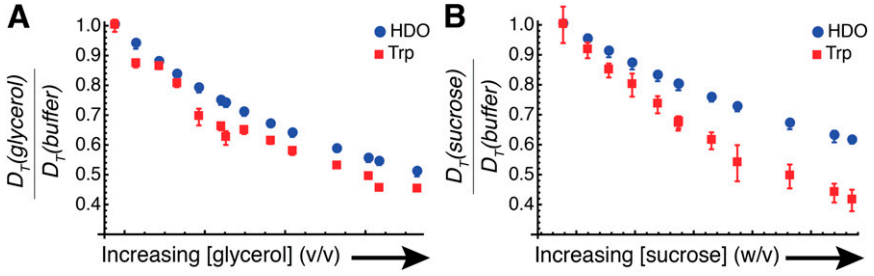

Fig. S4. Diffusion of water and tryptophan probes in viscogen solutions. (*A*) Diffusion coefficients of water and tryptophan as a function of added viscogen glycerol. (*B*) As in *A*, using the viscogen sucrose.

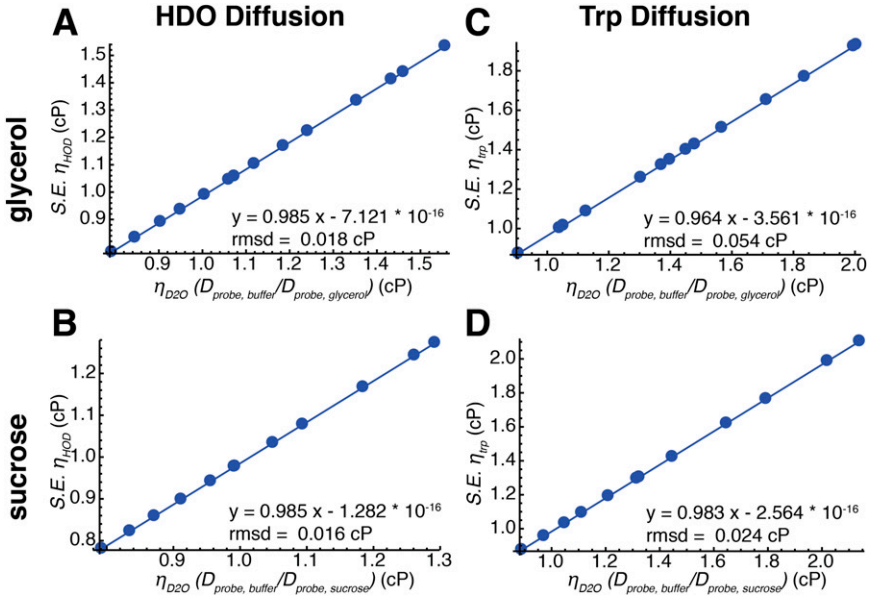

Fig. S5. Identical viscosity measures from different approaches. Correlation between solution viscosities measured from the diffusion of water or tryptophan for different concentrations of the viscogens glycerol and sucrose. Viscosity values were calculated from the diffusion coefficients of water (R_H = 1.12) or tryptophan (R_H = 3.88) using the Stokes–Einstein relation (*y*-axis) or from the relation $\eta_{probe} = \eta_{D2O}\frac{D_{probe,buffer}}{D_{probe,viscogen}}$, using the tabulated value for η_{D2O} at 45 °C (*x*-axis). See *SI Materials and Methods* for further details. Linear correlation plots are shown for viscosities obtained using water as a probe in viscogen solutions of glycerol (*A*) or sucrose (*B*), with similar plots obtained for the probe tryptophan in *C* and *D*.

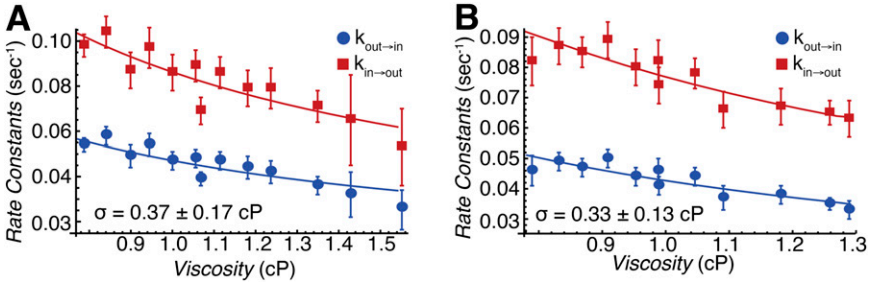

Fig. S6. Exchange rate constants $k_{out\rightarrow in}$(blue) and $k_{in\rightarrow out}$ (red) measured as a function of solution viscosity by using viscogens glycerol (*A*) and sucrose (*B*). Viscosity values were obtained from the relation $\eta_{probe} = \eta_{D2O}\frac{D_{probe,buffer}}{D_{probe,viscogen}}$ by using HDO as the probe. Fitted values of σ (using Eq. **1**) are in excellent agreement with those obtained when η values are calculated from water diffusion using the Stokes–Einstein equation.

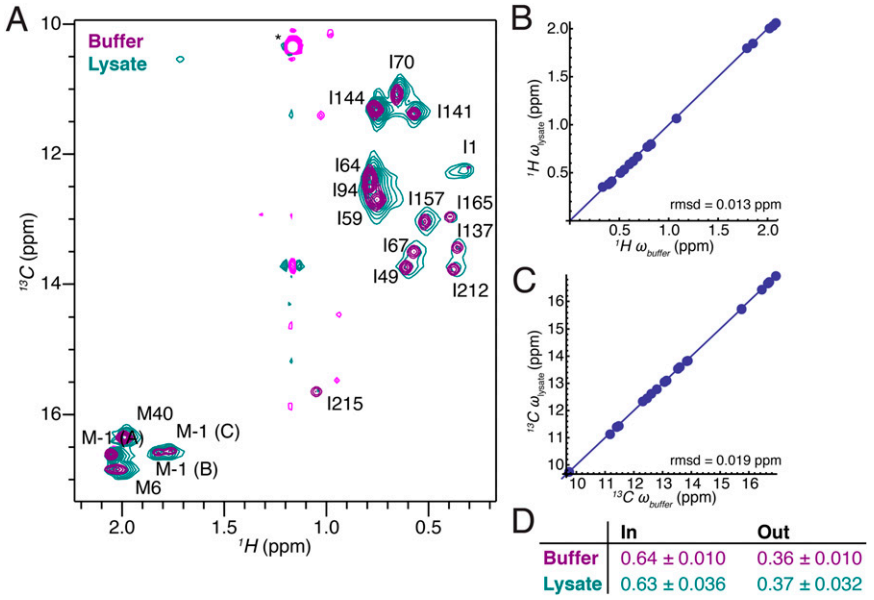

Fig. S7. The structure of α_7 is not perturbed by *T. thermophilus* lysate, 100 g/L protein concentration. (*A*) Two-dimensional ^{13}C,^{1}H HSQC spectra of U-^{2}H, $^{13}CHD_2$-M, $^{13}CHD_2$-I(δ1) M1I α_7 (purple contours) and lysate (cyan contours) recorded at 14 T and 45 °C. Correlation plots of ^{1}H (*B*) and ^{13}C (*C*) methyl group chemical shifts in lysate vs. buffer. The solid line is y = x, and the rmsd of α_7 methyl shifts is given in the lower right corner. (*D*) Relative populations of in and out states in buffer and lysate.

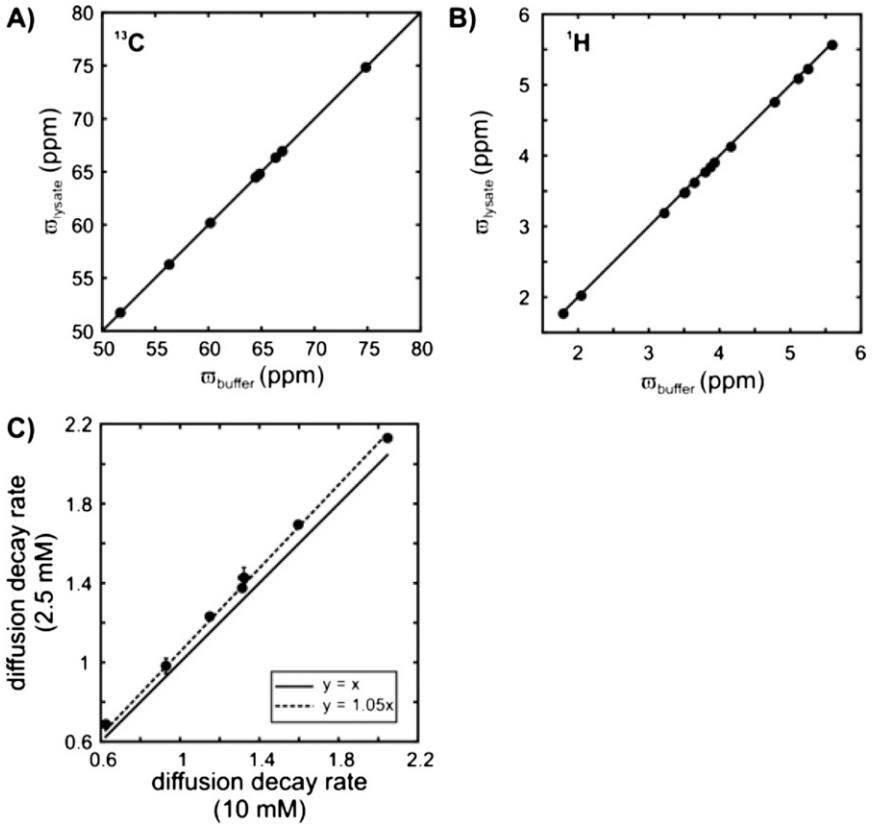

Fig. S8. Small molecule probes do not interact with the lysate. Linear correlation plots between (*A*) ^{1}H and (*B*) ^{13}C chemical shifts of small molecule probes in buffer (*x*-axis) and in 100 g/L *T. thermophilus* lysate (*y*-axis), 45 °C. (*C*) Correlation between diffusion decay rates of probes at 2.5 mM and 10 mM concentrations in 100 g/L *T. thermophilus* lysate. Solid lines in all panels are graphs of y = x, whereas the dotted line in *C* is the best fit of data points to an equation of the form y = mx.